Material Properties and Shrinkage of 3D Printing Parts using Ultrafuse Stainless Steel 316LX Filament

Haijun Gong[1], Cameron Crater[1], Ana Ordonez[1], Craig Ward[1], Madison Waller[1], and Charles Ginn[1]

[1] *Georgia Southern University, Statesboro, GA 30460, United States*

Abstract. As a novel manufacturing methodology, 3D printing or additive manufacturing (AM) attracts much more attentions for complex structure fabrication, especially for manufacturing metal parts. A number of metal AM processes have been studied and commercialized. However, most of them are costly and less accessible. This paper introduces a material extrusion based 3D printing process for making austenitic stainless steel 316L part using a metal-polymer composite filament (Ultrafuse 316LX). The stainless steel 316L metal specimens are printed by a commonly used 3D printer loaded with Ultrafuse filament, followed by an industry standard debinding and sintering process. Tests are performed to understand the material properties, such as hardness, tensile strength, and microstructural characteristics, of the stainless steel 316L material. In addition, an artifact model is designed to estimate the part shrinkage after the debinding and sintering process. It is found that the stainless steel 316L part exhibits apparent shrinkage after sintering. But using the Ultrafuse filament for 3D printing could be an alternative way of making metal AM parts.

1 Introduction

As an innovative metal part manufacturing method, 3D printing or additive manufacturing (AM) has been widely used in aerospace, bio-medical, and robotics industries [1]. At present, popular metal AM technology includes direct metal laser sintering (DMLS), selective laser melting (SLM), laser cusing, laser engineered net shaping (LENS), and electron beam melting (EBM), etc., which all use metallic powder as raw materials [2]. These metal AM technologies are capable of producing complex structures and geometrical features directly from digital models (CAD), which are impossible to create using other methods. However, all these metal AM processes need to employ high energy sources, such as laser or electron beam, to melt the powder, which demand a high cost of production and equipment [3]. The rapid growth of metal AM not only revolutionizes the existing methods of manufacturing, but also promotes new economic processes for metal parts. An affordable metal AM or 3D printing process is highly desired for small business and university labs.

The BASF Ultrafuse 316LX metal filament is newly invented and introduced to the AM community. The filament is a metal-plastic composite with high load of metal content (> 80%). The filament has two size options, 1.75 mm and 2.85 mm in diameter, which fit for any open source fused deposition modeling (FDM) based 3D printers. The usage of Ultrafuse metal filament is the same as using a plastic filament. The filament is firstly heated to glass transition temperature and then extruded from the nozzle for printing a "green part". Users are eligible to customize the parameters and process theme to achieve a desired density or efficiency. After that, the green part is subjected to debinding process to remove the plastic contents to form a "brown part", followed by a sintering process to finalize the metal part, as shown in Figure 1. The debinding and sintering process is the same to the industry standard process for metal injection molding parts [4]. At present, there are few studies about using the BASF Ultrafuse 316LX filament. Hence, the objective of this research is to investigate the usage of this metal filament on a low-cost AM equipment (desktop-size 3D printer) and then characterize the part properties after a printing, debinding, and sintering process, in comparison with the parts made by other method (flat rolled stainless steel 316L alloy). The research outcomes will exhibit some insights on a promising low-cost metal AM process and its part quality.

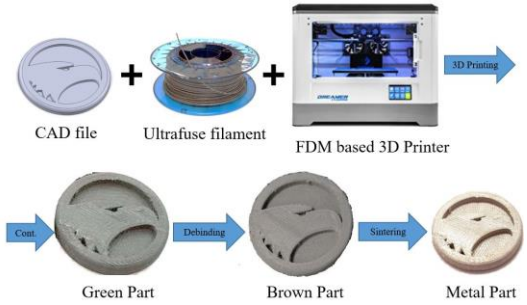

Figure 1. Schematic of metal 3D printing process using Ultrafuse filament.

2 Experimental Methods

The Ultrafuse 316LX filament is metal-polymer composite filament with a non-slip surface allowing its application in any Bowden or direct drive extruder. The filament with a diameter of 1.75 mm is acquired from BASF for this study. The equipment employed for printing Ultrafuse filament is a Flashforge Dreamer FDM-based 3D printer, which is used to print plastic filaments such as ABS, PLA, etc. BASF suggests a set of printing parameters for a generic 3D printer. Aiming to accommodate Ultrafuse filament to the 3D printer, experiment is conducted for investigating the optimum parameters, such as layer thickness, scan speed, extruder temperature, etc. The 3D printed samples (green part) is outsourced to DSH Technologies, LLC (Cedar Grove, NJ) for debinding and sintering of post processing. Catalytic debinding removes the polymer from the part and sintering in pure hydrogen or a vacuum results in the finished metal part. After being fabricated, the metal specimen's volume is measured using an AccuPyc 1340 gas pycnometer to estimate density and porosity, aiding to parameters optimization. The metal specimens are also sectioned, abrasively grinded and polished, and etched (Marble's reagent) for metallography. Microstructure is examined by an Olympus BX53M optical microscope. Tensile test specimens (rectangular cross section) are built in the *X-Y* orientation (ISO/ASTM 52921, 2013) using the optimum parameter set, conforming to ASTM E8 for tensile testing. Tensile tests were carried out using an ADMET tensile testing machine. A Rockwell hardness tester (B scale) is used for measuring the hardness of the sintered parts. An artifact model is designed using Solidworks with representative geometries in order to analyze the shape variations and shrinkage. A Keyence VR-3000 3D measurement system is used for the surface measurement of the artifact part.

3 Results and Discussion

3.1 Optimum Parameters

The experiment is carried out to investigate the optimum parameters of printing the green part using the Flashforge Dreamer 3D printer. The layer thickness, scan speed, and extruder temperature are greatly influential to the filament melting, extrusion, and deposition. Thus, these parameters are studied to optimize the recipe of printing process. The criterion of good printing is assessed by yielding a consistent thin strand, depositing in predetermined locations, and adhering to the solidified prior layer. As the voids are coherently included in the printed part, the FDM process is unable to build fully dense samples. The density is also assessed to help identify the optimum parameters. It is found that the layer thickness 0.2 mm, scan speed 60 mm/s, and extruder temperature 235 ºC are eligible to print a desired part, with consistent surface topography and laminations. The other parameters are set to be factory default. The green parts are then debinded and sintered to be the stainless steel 316L metal part. The density of the metal part is measured to be 7.88 g/cm^3, which is comparable to the typical stainless steel 316L alloy (8 g/ cm^3).

3.2 Microstructural Analysis

After debinding the plastic component from the green part, sintering is performed in the furnace to densify the metal component of the brown part. Within a pure hydrogen or a vacuum atmosphere, small grains are recrystallized and growing to form a set of strain-free and equiaxed grains. As shown in Figure 2, the austenitic stainless steel 316L alloy has grains of approximately equal dimensions in all directions. Because the grain size depends on both time and temperature of sintering. The grains are characteristic of the annealed condition without apparent dislocations. This implies that the sintered metal sample is softer and weaker, but more ductile. It is also noted that the grain morphology is independent of the orientation of building, unlike the SLM parts (anisotropy). Comparing the Figure 2 (a) and (b), there is no layer-effect along the building direction. All grains are uniformly allocated, which indicates an isotropic mechanical properties of the sintered stainless steel 316L part.

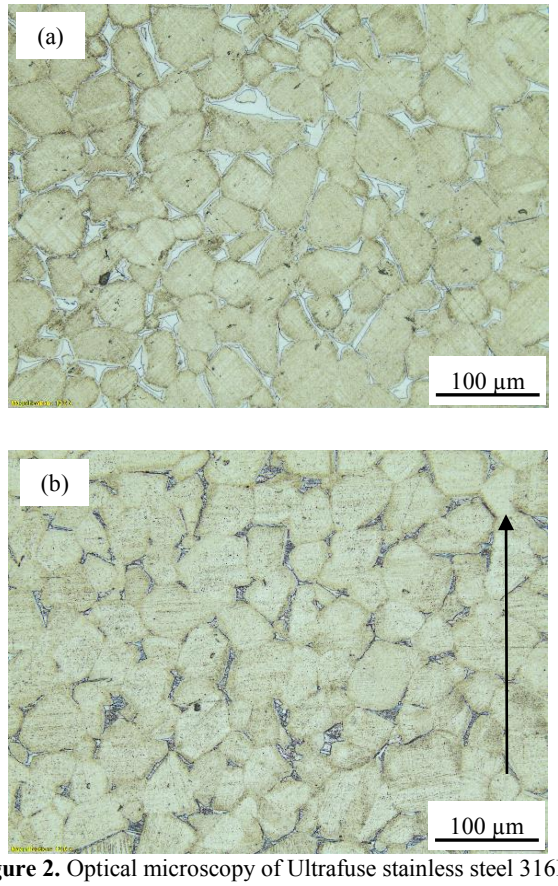

Figure 2. Optical microscopy of Ultrafuse stainless steel 316L microstructure after sintering, (a) horizontal cross section, (b) vertical cross section (arrow indicates building direction)

3.3 Tensile Strength and Hardness

Tensile test specimen is directly printed and then post-processed to be the metal part. The tensile property is exhibited via a stress-strain curve plotted using Microsoft Excel, as shown in Figure 3. The tensile specimen is so

ductile that the extensometer reached its limit without rupture. Hence, only part of the stress-strain curve is shown in Figure 3. It is noted that the specimen has been stretched to 20% but the stress is still climbing. The tensile test is completed after unloading the extensometer. Yield strength, ultimate tensile strength (UTS), elastic modulus are summarized in Table 1, in comparison with the flat rolled stainless steel 316L tensile properties (ASTM A240/A240M). The tensile property indicates the Ultrafuse stainless steel 316L alloy has a lower yield strength, UTS, and elastic modulus, which are attributed to its grain size and austenitic microstructures. As shown in Figure 4, it can be seen that the hardness value is identical in both horizontal and vertical directions, even though there is a minor statistical variation as specified by the error bar. This result conforms to the isotropic microstructure along both horizontal and vertical directions in Figure 2. The hardness value is less than the flat rolled stainless steel 316L (95 HRB), in agreement with its dislocation-free microstructure.

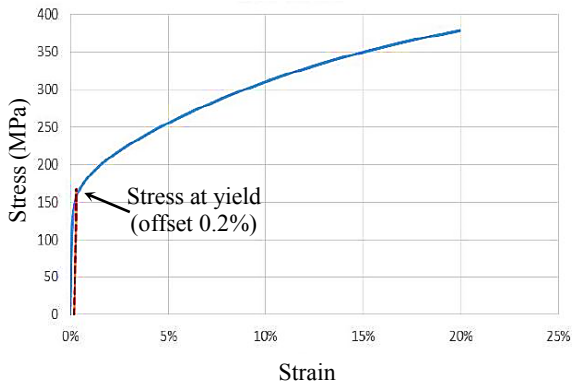

Figure 3. Stress-strain curve of Ultrafuse stainless steel 316L alloy.

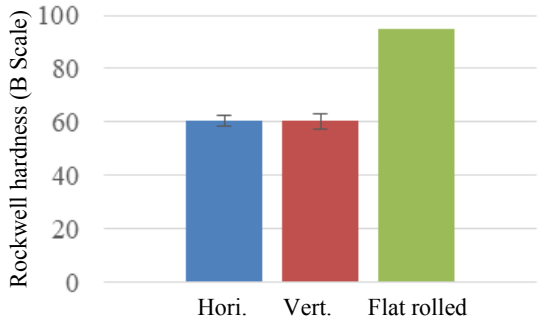

Figure 4. Rockwell hardness (B scale) test results.

Table 1. Tensile Properties of Ultrafuse stainless steel 316L alloy and flat rolled stainless steel 316L alloy.

	Ultrafuse SS 316L	Flat rolled SS 316L[a]
Yield Strength (MPa)	167	170
UTS (MPa)	436	485
Young's Modulus (GPa)	152	193

[a] www.azom.com

3.4 Shrinkage

The artifact model is printed for shrinkage analysis, as shown in Figure 5. The CAD model has a set of features of interest (FOI) marked with sequence number. A couple of side holes are designed with multiple geometries to verify that the un-supported features are printable. Figure 5(b) shows the green part of the artifact which is directly printed using Ultrafuse filament. It is noted that all the un-supported features are printable. This demonstrates that the extruded filament has a great shape retention due to the fast phase transformation from viscous state to solid state. It also confirms that the extruder temperature 235 ºC is at an appropriate condition higher than the glass transition temperature of the Ultrafuse filament. The green part is measured using Keyence VR-3000 to the FOIs before being sent out for debinding and sintering. A surface morphology measurement of green part is illustrated in Figure 5 (c). The metal part (sintered part), which is shown in Figure 5(d), is also measured using the same equipment to compare with the FOIs of the green part for estimating the shrinkage.

Metal part has the similar shape characteristics but a decreased size due to the shrinkage. The major FOIs maintain the geometrical configuration features. This ensures that the FDM based metal AM is capable of making metal part using Ultrafuse filament, as long as the shrinkage is compensated when printing the green part. The size of FOIs in *X*-*Y* plane (diameter, edge length, etc.) and along *Z*-axis (height, depth, etc.) are of great interest in this study. The diameter of FOI #1-3, #7-9 and the edge length of FOI #4-6 are compared between green part and metal part, as shown in Figure 6 (a). The comparison of the height of FOI #1-2, #4-9 and the depth of FOI #10-11 are illustrated in Figure 6 (b).

It can be seen that FOI #1-3 have the same circular feature but different size. The FOI #1 is the largest circular feature whose nominal size is 15 mm. Its shrinkage rate is about 14%, in comparison with FOI #2 and #3 with the shrinkage rate of ~18%. FOI #7-9 have the same circular feature and size (nominal size 4 mm), whose shrinkage rate are nearly the same, approximately ~13%. FOI #4-6 have square feature at different levels along *Z*-axis. The shrinkage rate is ~13%, ~16%, and ~17%, respectively. This exhibits an interesting phenomenon that the feature shrinkage in *X*-*Y* plane is slightly influenced by its *Z*-axis level. A feature at a lower level has less shrink than the same feature at a higher level.

The comparison of the height of FOI #1-2, #4-9 and the depth of FOI #10-11 is conducted along *Z*-axis. The shrinkage of FOI #1's height is about 23%, which is larger than FOI #2 (~20%). FOI #4 and #5 have the similar shrinkage ~22% in height, in comparison with the shrinkage of ~19% of FOI #6. There are no apparent variations of the height shrinkage of FOI #7-9, about 23-24%. As for the depth shrinkage, FOI #10 has a shrinkage of ~18%, compared to ~15% of FOI #11. It is noted that a larger height or depth variation tends to occur at a lower level along *Z*-axis. Overall, the calculated shrinkage rate along *Z*-axis shows a higher percentage than the geometrical features in *X*-*Y* plane. This could be

attributed to the effect of metal component gravity during the sintering process.

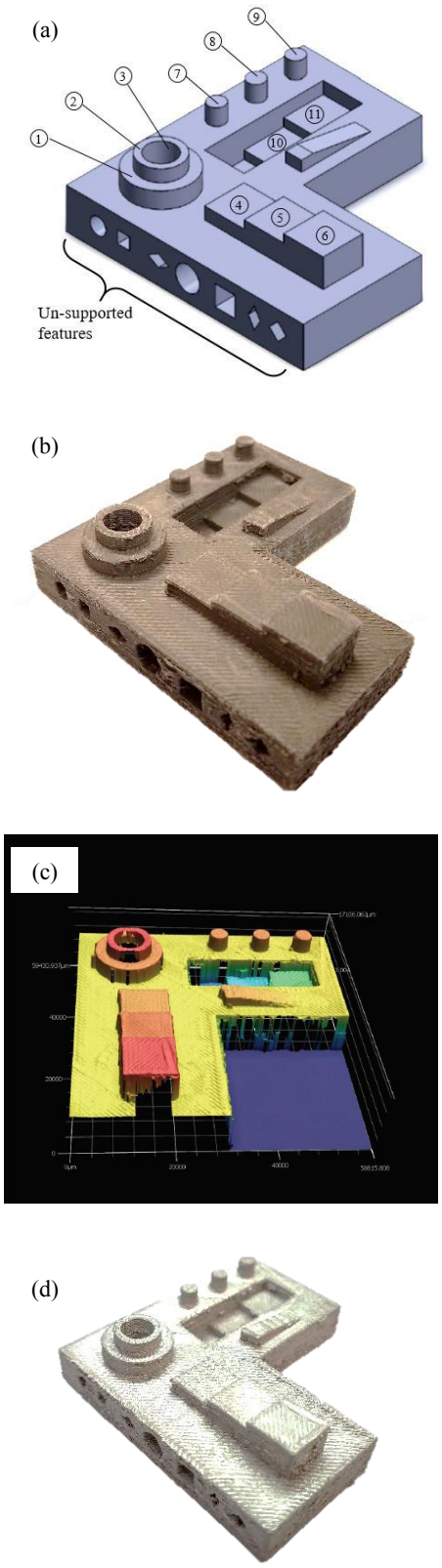

Figure 5. Artifact for shrinkage analysis, (a) CAD file, (b) green part, (c) surface measurement of green part (d) metal part.

In general, the calculated shrinkage rate indicates that the geometrical features in *X*-*Y* plane exhibit a size reduction of 13-18%, while the shrinkage along *Z*-axis shows a higher percentage of 18-23%.

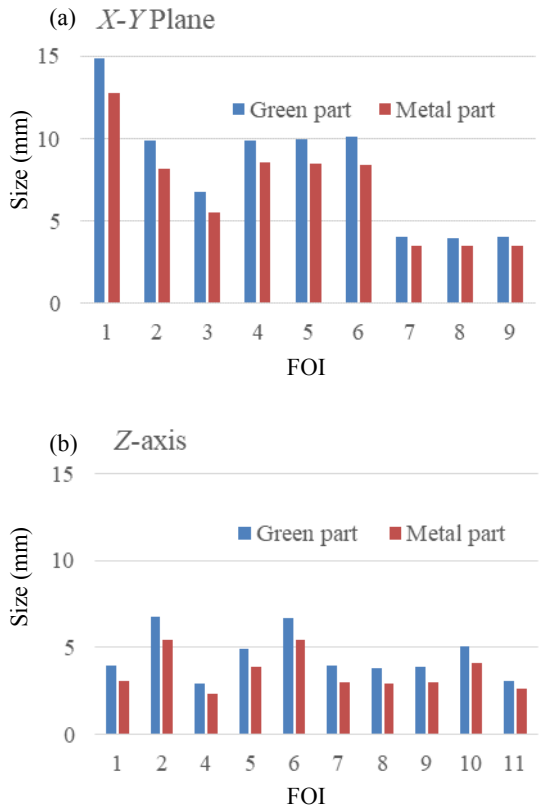

Figure 6. Size comparison of FOIs, (a) in *X*-*Y* plane, (b) along *Z*-axis.

4 Cost Analysis

Equations should be centred and should be numbered with the number on the right-hand side. (Delete) There are many benefits of using Ultrafuse filament for metal 3D printing parts, compared to other metal AM processes. The investment for hardware and materials is low. The FDM-based 3D printer is easily operated and maintained by users. The price of metal filament is affordable and more easy-handling than metallic powders. For instance, a couple of kilograms of metallic powder usually needs to be loaded into a SLM machine to start a build. The un-melted powder is sieved and recycled for next build. But metal filament is only needed by the required quantity to start a printing, i.e. use as needed. 3D printer is immediately ready for next build when the green parts are completed and removed for post processing. This extremely reduces the lead time for machine cleaning and material recycling. Moreover, the metal filaments is used for printing in an open chamber at room temperature, compared to the SLM process (inert gas filled chamber) and EBM process (vacuumed chamber) [5]. Also, the maintenance of a FDM 3D printer, debinding, and sintering equipment are less expensive than the laser or electron based metal AM system. This shows a substantial cost advantage to produce metal AM parts.

5 Conclusion

This study introduces an Ultrafuse 316LX filament for metal 3D printing. The process is faster and less expensive than the existing powder-bed-fusion based metal AM technology. The microstructure of the austenitic stainless steel 316L alloy consists of strain-free and equiaxed grains. The tensile strength and hardness are examined and compared with the flat rolled stainless steel 316L. It is also found that the shrinkage rate from green part to metal part varies in *X*-*Y* plane and along *Z*-axis. But using the Ultrafuse filament for 3D printing is a promising way of making metal AM parts and deserves further investigations, due to its cost efficiency.

References

1. J. J. Lewandowski, M. Seifi, Ann. Rev. Mater. Res. **46**, 151-86 (2016)
2. I. Gibson, D. W. Rosen, B. Stucker, *Additive manufacturing technologies: rapid prototyping to direct digital manufacturing* (Springer, 2009)
3. D. S. Thomas, S. W. Gilbert, NIST Special Publication 1176 (2014)
4. A. Páez-Pavón, A. Jiménez-Morales, T. G. Santos, L. Quintino, J. M. Torralba, J. Magn. Magn. Mater. **416,** 342-7 (2016)
5. H. Gong, K. Rafi, H. Gu, G. D. J. Ram, T. Starr, B. Stucker, Mater. Design **86,** 545-54 (2015)